Emergence of single-particle mobility edge (SPME) in a ladder network under a modified Aubrey-Andre-Harper (AAH) kind distortion

Arpita Goswami*

Indian Institute of Technology Tirupati, India, 517619

This research examines the localization and delocalization phenomena in a two-strand ladder network incorporating a generalized Aubrey-Andre-Harper (AAH) model in different parametric regions. In our model, we have introduced a distortion that is neither periodic (Bloch-type) nor random (Anderson-type) but instead has a slowly varying pseudorandom pattern described by $\Gamma_n = \lambda cos(2\pi Q n^\nu)$, where $0 < \nu < 1$. We have demonstrated that in the generalized ladder network in the $0 < \nu < 1$ limit, it is not possible to see a pure metal-insulator transition due to the presence of a single particle mobility edge (SPME) state. We have shown that at $\nu = 0.908$ (and in its immediate neighborhood), the energy states maintain delocalization up to a considerable distortion strength and that a pure metal-to-insulator transition occurs at $\nu = 1$ as λ increases. We have also demonstrated the phase diagram for the ladder network in the parametric region ν-λ. We extensively studied wave packet dynamics by examining different quantities to establish the claim satisfactorily. We also have studied the multifractality of the quantum network. These findings suggest that this ladder network could serve as a valuable platform for investigating the interplay between localized and extended states.

I. INTRODUCTION

The Aubry-Andre model [1] is renowned for its simplicity and rich electronic and topological transport properties, which constitute a central area of interest in condensed matter physics. The periodic incommensurate [2–7] diagonal term renders it a significant subject for researchers investigating quantum phase transitions (QPT). This non-interacting nearest-neighbor hopping model exhibits a symmetric spectrum about zero energy and demonstrates self-duality, extending to the localization transition at a critical point [8]. The symmetric property of the spectra is eliminated in the presence of non-hermiticity [9–11], next-nearest neighbor hopping [12], and quasiperiodic site energies [13, 14]. In addition to theoretical studies, numerous experiments have been conducted to realize this model. It has been implemented in ultracold atoms [15, 16], photonic crystals [17], and polariton condensates [18]. The experimental realization of the quantum critical phase transition has recently been reported in a generalized Aubry-Andre model with superconducting circuits [19]. The mobility edges [4, 5, 20–22] can be characterized as the coexistent state of delocalized and localized phases, facilitating understanding of electronic properties in disordered systems. The self-duality of the one-dimensional (1D) Aubry-Andre model [1, 23] under the Fourier transformation at the critical quasiperiodic potential [24], which induces the quantum phase transition, is a well-established phenomenon. In the Aubry-Andre model, the transition occurs without mobility edges. However, the generalized [5, 21] Aubry-Andre (or SSH) model exhibits a self-duality relation with mobility edges for a fixed incommensurate potential strength. Recently, a self-duality

with exact mobility edges has been reported in a two-dimensional non-Hermitian [9, 10] quasicrystal model with parity-time symmetry. The mobility edge system demonstrates a notably high thermoelectric effect, which has potential applications in thermoelectric devices. In a non-equilibrium setting, quantum phase transitions can be observed under the effect of a quench. The study of quantum quench involves the abrupt change in system parameters. If this abrupt change governs time evolution, it leads to dynamical quantum phase transitions (DQPTs), which the non-analyticity of the Loschmidt echo can probe. A Loschmidt echo represents the ground state's survival probability during the initial state's time evolution. This measure is particularly significant for defining non-equilibrium phase transitions. This quenching occurs in atomic Mott insulators, Aubry-Andre models, the Lipkin-Meshkov-Glick model, standard Anderson models, and other systems. DQPTs were achieved under the quench dynamics of out-of-time-ordered correlators in a recent experimental configuration of a nuclear magnetic resonance simulator.

The one-dimensional Anderson model does not have the metal-to-disorder transition because all single-particle states can be localized with minimal potential. However, the aforementioned transition can be observed in the parameter space's 1D Aubry-Andre-Harper (AAH) model. This transition can be observed for specific criteria (h = 2t) between the values of hopping strength (t) and the onsite potential's strength (h). However, the eigenstates at the transition points can be characterized neither as extended nor localized states. Consequently, states at that point can be termed critical. The system is expected to exhibit a broad range of different exponents at this point. This property of the system that demonstrates the aforementioned behavior is also known as multifractality. In recent years, AAH modulation studies have received considerable scholarly attention. Most of
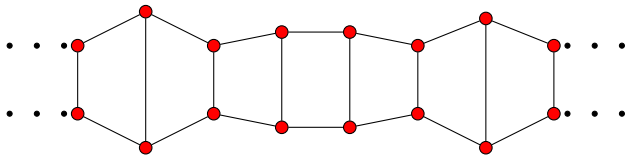
FIG. 1: Schematic diagram for a two-strand ladder network with random modulation

these studies are confined to purely one-dimensional systems with no width. A recent study used minimal
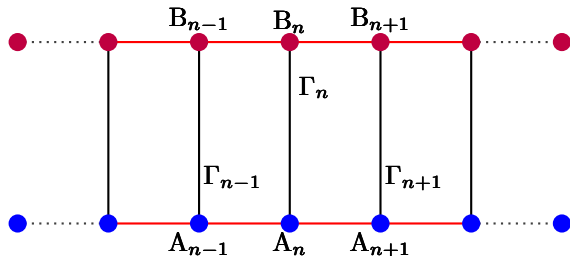

FIG. 2: Schematic diagram for a two-strand ladder network

width using a geometrically distorted ladder (GDL) [25]. The geometrically distorted ladder (GDL) with deterministic distortion was achieved by assigning different hopping parameters along the ladder's rungs. We extended this work by introducing a general GDL along the rungs. The additional motivation for selecting this topic for investigation is understanding the dynamics of an isolated quantum system. A primary question that has been extensively studied for decades is whether a generic isolated quantum many-body system can achieve thermalization under its own dynamics. It is generally posited that an interacting many-body system may fail to thermalize through its own dynamics if it is not coupled to any external bath (closed system) in the presence of strong disorder [26–28]. The failure of thermalization results in a nonthermal phase, also known as stable dynamical non-ergodicity at a finite energy density (nonzero temperature). This phenomenon is referred to as many-body-localization (MBL) [29–31]. One characteristic of the MBL phase is that it significantly violates the eigenstate thermalization hypothesis (ETH) [32, 33]. From an experimental perspective, some quantum many-body systems exhibit strong isolation from the environment, such as ultra-cold atoms [34] and trapped ions [35]. An important inquiry is what occurs in a system when coupling is introduced between localized and extended degrees of freedom in a many-body system. Moreover, if the bath is small compared to the system size, whether the system will thermalize becomes a non-trivial question. This question can be reformulated as follows: Does an MBL system thermalize if coupled with one possessing completely ergodic states and a comparatively smaller system size? The key question is whether the MBL sys-

tem will localize the bath or if the bath will thermalize the MBL states. Despite extensive theoretical [26–31, 36] and experimental studies [37–39], the question remains unresolved. The possibility of achieving a system that coexists with MBL and ETH states remains controversial. This coexistence can potentially lead to a state known as the nonergodic metallic phase [40, 41], which exhibits properties of both MBL and ETH. Some numerical results indicate that the aforementioned phase can be observed under certain conditions, while others suggest the existence of a many-body mobility edge (implying that the system contains MBL states up to a certain energy level, beyond which it contains ETH states). Recent work has argued that obtaining a many-body mobility edge in a truly random disorder system within the thermodynamic limit is impossible due to rare-region effects [42, 43]. It is noteworthy that the mobility edge allows the system to function as its own bath at finite temperature; the extended states exchange energy with the MBL states and ultimately act as a bath for those MBL states.

Our model can be considered two tight-binding models coupled via an aperiodic and deterministic modulation. So it is interesting to see whether the presence of this kind of distortion fully localizes the states or the extended states of a tight-binding type system will be able to act like a bath for the system and help the system to thermalize (keep the states extended in single-particle limit), or the system gives rise to SPME. So, our model can be considered one of the potential testing grounds for studying the emergence of nonergodic intermediate phases in a 2D model.

The main focus of our study is to motivate the experimental studies to establish the stability of SPME in this system. Eventually, it can be particularly useful in future investigations of non-ergodic metallic phases. In this paper, we discuss one modified version of the geometrically distorted ladder. Here, we have introduced generalized deterministic distortion, which depends on the site index. Moreover, the distortion is generalized with the help of one parameter; we studied the limiting case behaviors. In this paper, we will see how the introduction of uneven hopping and generalization of distortion changes the system's wave function dynamics.

The paper is presented as follows. In section (II), we define the system and its corresponding Hamiltonian. In sections (III, III B,), we discuss localization and delocalization of the model using the inverse participation ratio (IPR) and discuss the multifractal nature of the transition point (or critical point). In section (IV), we will discuss the dynamical properties of the wavepacket by calculating the spread of the wavepacket using mean square displacement (MSD), time-dependent IPR, return probability (RP), and information entropy (IE). To check the robustness of the presence of SPME, we studied the variation of MSD and IE in a sufficiently large time limit. In section (V), we conclude our discussion.
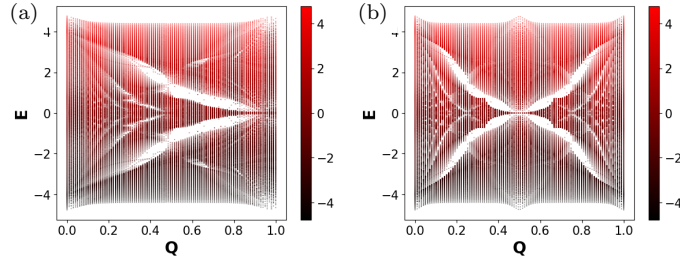
FIG. 3: (a) Energy as a function of Q, (b) Energy as a function of Q for $\nu = 0.908$ and $\nu = 1$ respectively
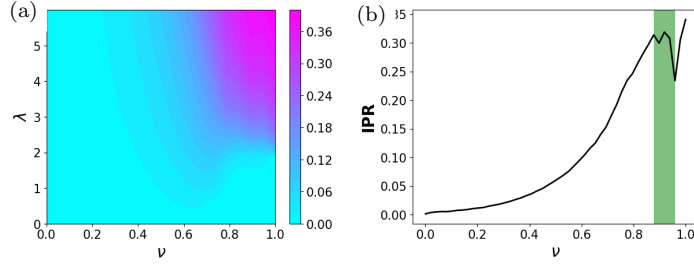

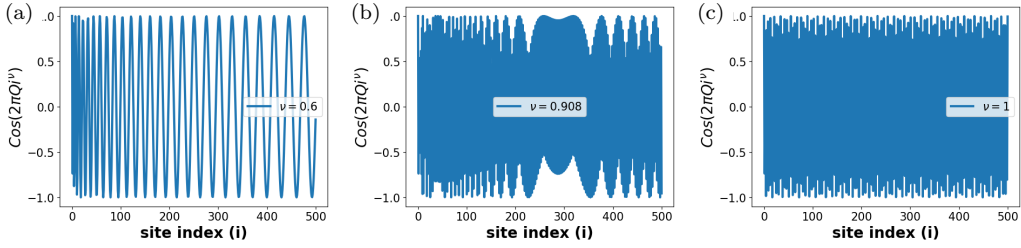FIG. 4: (a) Phase diagram of the model in fig 1, (b) IPR vs. ν at $\lambda = 4$

FIG. 5: (a), (b), and (c) are the plots of the variation of potential $cos(2\pi Q n^\nu)$ over sites for $\nu =$ 0.6, 0.908, and 1, respectively
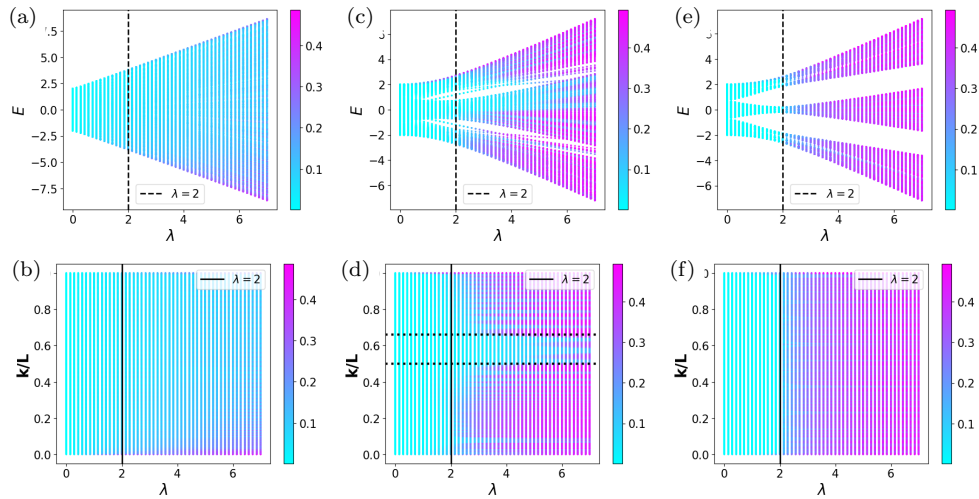

FIG. 6: (a)-(b), (c)-(d), and (e)-(f), are the plots of IPR density with E and λ and the IPR density plot with respect to energy level index $\frac{k}{L}$, and λ respectively, for $\nu =$ 0.6, 0.908, and 1
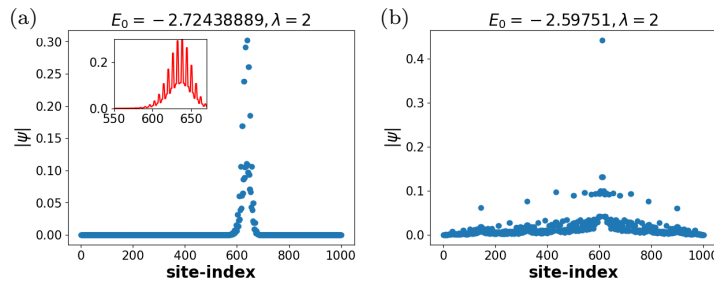
FIG. 7: $|\psi|$ of ground state wave function vs. site index for (a) $\nu = 0.908$ and (b), $\nu = 1$ respectively

II. MODEL AND HAMILTONIAN

A ladder with a completely random geometrical disorder can be visualized as Fig. (1). For simplicity, we have drawn the system schematically in the following Fig. (2), which we will study in detail in the following sections. In this model, we have two types of hopping. One is nearest-neighbor hopping (horizontal) with strength 't' between n^{th} and $(n+1)^{th}$ sites of every arm (A and B) of the ladder. Another is vertical hopping, which takes place between the nth sites of two arms (A to B), modulated by $\Gamma_n = \lambda cos(2\pi Q n^\nu)$ the hopping between the nth sites. The Hamiltonian can be written as

$$H = t \sum_n (A_{n+1}^\dagger A_n + B_{n+1}^\dagger B_n) + \epsilon \sum_n (A_n^\dagger A_n + B_n^\dagger B_n) + \Delta_1 \tag{1}$$

where $\Delta_1 = \sum_n \Gamma_n(A_n^\dagger B_n + B_n^\dagger A_n)$ and $\Gamma_n = \lambda cos(2\pi Q n^\nu)$.

So, as we can see, the vertical modulation is neither random nor periodic but is a quasiperiodic type but does not belong to the simple incommensurate class. The modulation is aperiodic and deterministic and slowly varying, which is expressed as

$$\Gamma_n = \lambda cos(2\pi Q n^\nu)$$

where Q is a real number (which can be rational and irrational), but in our work we have taken $Q = \frac{\sqrt{5}-1}{2}$ so that $\nu = 1$ we can recover Harper's equation [44]. In our work, we have used the value of the exponent ν to be between 0 and 1, and the λ ranges from 0 to 6. In our calculation, we kept the onsite potential (ϵ) term zero. We take the size of the system to be N = 1002.

III. DIFFERENT MEASURES FOR PROBING METAL-INSULATOR TRANSITIONS

A. Characterizing different phases with IPR

Before going into the detailed discussion of the localization-delocalization character of the above variant of quantum networks, we will try to see the distribution of energy eigenvalues of the system as a function of Q.

We have demonstrated the famous Hofstadter butterfly structure at $\nu = 0.908$ and $\nu = 1$ respectively in Fig. 3, which represents the multifractality of the energy spectrum of the corresponding quantum networks. The white spaces in the graph are energy gaps, where no allowed energy states exist. These gaps separate energy bands and reflect the topological nature of the system. We can observe that the butterfly structure is appreciably different in both $\nu = 0.908$ and $\nu = 1$. In the case of $\nu = 1$, we see a well-symmetric band structure maintaining reflection symmetry where we can see many landau subbands (symmetric about Q = 0.5 and E = 0 axis). We can even observe the energy gaps in the fractal pattern. But for $\nu = 0.908$, the reflection symmetry of the band structure about Q = 0.5 axes vanishes, which represents that at this value of ν, the square lattice (ladder network) loses inversion symmetry. As a result, the butterfly structure at $\nu = 0.908$ is appreciably deformed from the actual butterfly structure. In the energy interval [0, 2] and [-2, 0], wide band gaps can be observed for $\nu = 0.908$, and at $\nu = 1$, the gaps vanish. Multifractality often arises at the transition between localized and extended states in quantum systems, such as in the metal-insulator transition. To understand the transition more precisely, we will discuss the other quantities. One can numerically calculate the inverse participation ratio (IPR) and the normalized participation ratio (NPR) for the explicit verification of the metal-insulator transition. These two quantities are considered to be more robust theoretical tools for understanding the Anderson transition. For a single-particle system, IPR can be defined as follows:

$$IPR = \frac{\sum_{i=1}^N |\psi_i|^4}{(\sum_{i=1}^N |\psi_i|^2)^2} \tag{2}$$

where ψ_i is the normalized eigenstate of the system's Hamiltonian, so $\sum_{i=1}^N |\psi_i|^2 = 1$. For extended (or delocalized) state IPR is of the order of $\frac{1}{\sqrt{N}}$ this eventually goes to zero in thermodynamic limit. On the other hand, this approach to unity when all the states are localized.

NPR is a complementary quantity of IPR, which takes the unity value for the extended state and the zero value for the localized state in the thermodynamic limit. The
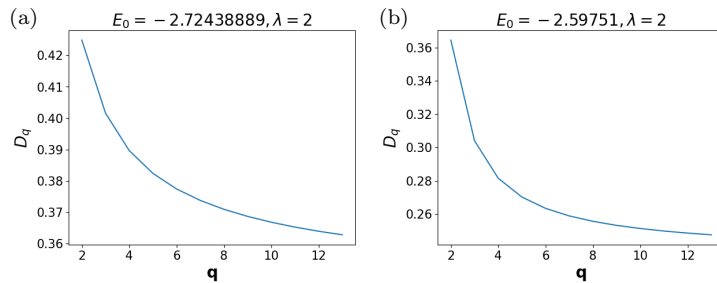
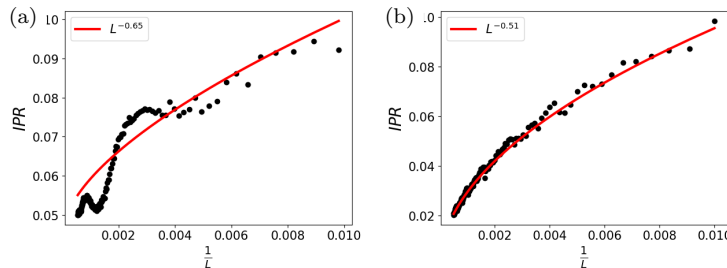FIG. 8: D_q vs. q for (a) $\nu = 0.908$ and (b) $\nu = 1$ respectively

FIG. 9: Scaling property of IPR at (a) $\nu = 0.908$ and (b) $\nu = 1$ respectively

NPR can be defined as follows:

$$NPR = \frac{1}{N \sum_{i=1}^{N} |\psi_i|^4} \qquad (3)$$

where N represents system size. Now we see in our Hamiltonian there are three parameters: One is t, which is the magnitude of horizontal hopping; one is λ, which gives the magnitude of the distortion; and the last one is the exponent ν. For the sake of simplicity, we keep $t = 1$ throughout our calculation. For checking the system's behavior on the parameter space ν and λ, we have demonstrated the phase diagram in Fig. 4 by plotting IPR as a function of ν and λ. We can see that for $\nu = 1$ exactly at $\lambda = 2$, there is a phase transition. For a very low value of ν, the value of IPR always remains almost 0 (at all values of λ), representing no strong metal-to-insulator phase transitions at those values. Now, what happens to the system in the limit $0 < \nu < 1$, to see that we have plotted the IPR as a function of ν at a high value of distortion strength $\lambda = 4$. In Fig. 4, we can see the IPR starts decreasing near $\lambda = 0.878$ and again starts increasing, beyond $\lambda = 0.97$ showing the indications of the reentrance of delocalized states in that region. Now we have chosen three points $\nu = 0.6$, $\nu = 0.908$ (one of the dips of IPR at large λ 4), and $\nu = 1$ to see their corresponding density plots of IPR (Fig. 6), wherein the upper panel, we can see that the density of IPR values has been plotted as a function of λ in those three ν limits. In the lower panel, IPR has been plotted with respect to the normalized energy index $\frac{k}{L}$. In Fig. 6a, we can see that the IPR value is not changing even with the increase in the λ value for $\nu = 0.6$; the corresponding IPR vs. nor-

malized energy index $\frac{k}{L}$ plot (Fig. 6b) agrees with this result. Now, when we increase the value ν to 0.908, a pure metal-insulator transition is impossible, as Fig. 6c and 6d suggest that the middle energy states remain delocalized. Fig. 6e and 6f suggest that for $\nu = 1$, there is a pure transition from delocalization to localization exactly at $\lambda = 2$.

To understand this, we can see Fig. 5, which explains how the potential varies over the site index. We see at $\nu = 0.6$, the potential is fully periodic, and at $\nu = 1$, the potential is quasi-periodic in nature. The point $\nu = 0.908$ point shows neither completely periodic nor completely quasi-periodic. So, this point is supposed to show some exclusive phenomena that differ from both the limiting cases. Distortions as low as $\nu = 0.6$, are not enough to get a metal-insulator transition in 2D.

B. Multifractality

The generalized inverse participation ratio is a multifractal scaling analysis used for Anderson transitions. For a single-particle quantum state $|\psi\rangle$, the generalized inverse participation ratio can be defined as

$$IPR(q) = \sum_{i=1}^{L} |\langle I|\psi\rangle|^{2q} = \sum_{i=1}^{L} |c_i|^{2q}, \qquad (4)$$

where q is a real number. We are restricted to the $q > 0$ region in our discussion, although $q \leq 0$ is also studied in the literature. Also, we are focused on the average over-trajectory discussion. q can also be considered a moment.
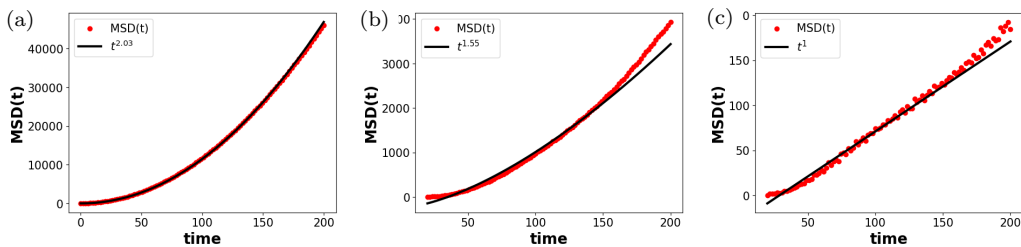
FIG. 10: (a), (b), and (c) are the plots of mean square displacement as a function of time for $\lambda = 0.5$, 2, and 4, respectively, for $\nu = 0.908$
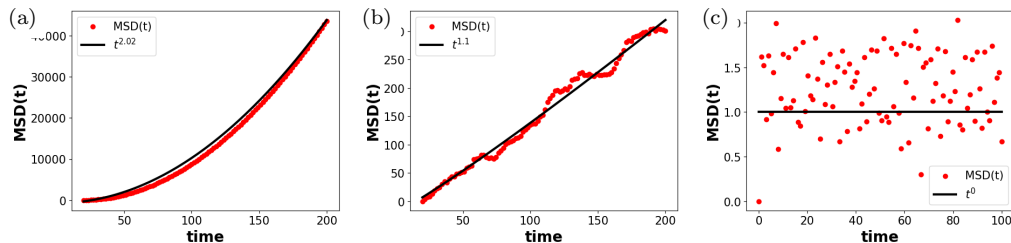

FIG. 11: (a), (b), (c) are the plots of mean square displacement as a function of time for $\lambda = 0.5$, 2, 4 respectively for $\nu = 1$

The quantity I_q is known to have anomalous scaling behavior. $I_q \equiv N^{-\tau_q}$, where $\tau_q = D_q(q - 1)$ this D_q is the fractal dimension. For a completely localized state, $D_q = 1$; for a completely delocalized state, $D_q = 0$ irrespective of the q value. When D_q takes a constant value between 0 and 1 for all q values, the state will be called a fractal state with one fractal dimension. If D_q is between 0 and 1 but depends on the moment q, then that state will be called multifractal. We investigated the multifractal behavior of the eigenstate in the critical region ($\lambda = 2$) for $\nu = 0.908$ and $\nu = 1$ points. The fractal dimension D_q is also plotted against q in Fig. 8. It can be seen from the graph that the fractal dimensionality decreases with moment q. Fig. 7 represents the distribution of the multifractal ground state with energy $E_0 = -2.72438889$ corresponds to $\nu = 0.908$ and $E_0 = -2.59751$ which corresponds to $\nu = 1$ respectively. So, by seeing the ground state distribution and the D_q vs. q graph, we can tell that the corresponding network is multifractal in that critical region. Next, we will discuss the scaling behavior of the IPR with different system size N when the system is at its critical region $\lambda = 2$ for $\nu = 1$ and $\nu = 0.908$ in Fig. 9. For completely delocalized regions, IPR decays with system size as L^{-1}; conversely, if the IPR is independent of L or varies as L^0, that represents completely localized regions. In Fig. 9, we can see that for $\lambda = 2$ (critical region) and $\nu = 1$, the decay is of the order of $L^{-0.51}$ and for $\nu = 0.908$ IPR varies as $L^{-0.65}$, In both cases, we saw that the IPR goes as L^x where $-1 < x < 0$, so that's why the corresponding regions of power law variation of IPR are called multifractal regions.

IV. DYNAMICS OF GROUND STATE WAVE FUNCTION

At any arbitrary time t (time evolution of wave function), the electronic wave function can be constructed as follows:

$$\psi(t) = \sum_n C_n e^{-iE_n t} |\psi_n(0)\rangle, \tag{5}$$

where $|\psi_n(0)\rangle$ represents an electronic wave packet at time $t = 0$, which can be expressed as follows:

$$\psi(t) = \sum_n C_n(0) |\psi_n(0)\rangle \tag{6}$$

where $C_n(0)$ expresses the probability amplitude of finding the particle at time t = 0 at n^{th} site. If the electron is initially localized at the mth site, then the amplitude can be expressed as:

$$C_n(0) = \langle \psi_n(0)|m\rangle.$$

Now, we will study the different dynamical probes for characterizing the transition and the different phases (localized or delocalized).

A. Time dependence of mean square displacement

If we consider the electron to be at the mth site initially, then the spread of the wave function at any time
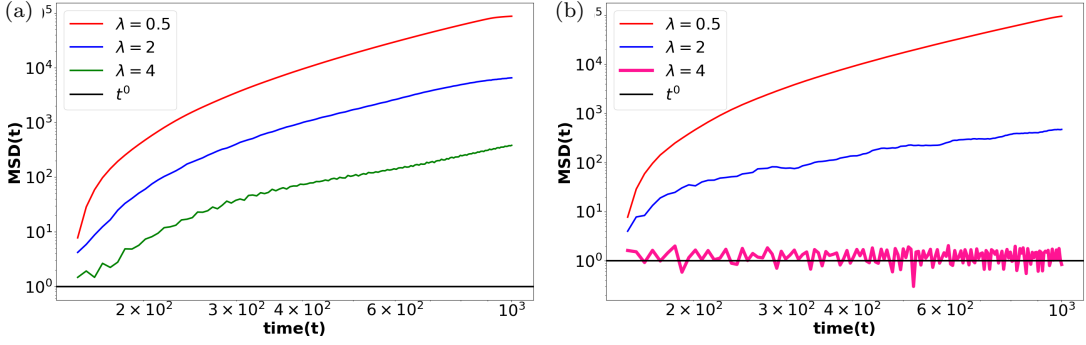
FIG. 12: (a), (b) are the plots of mean square displacement as a function of (long) time for $\nu = 0.908$, $\nu = 1$ respectively
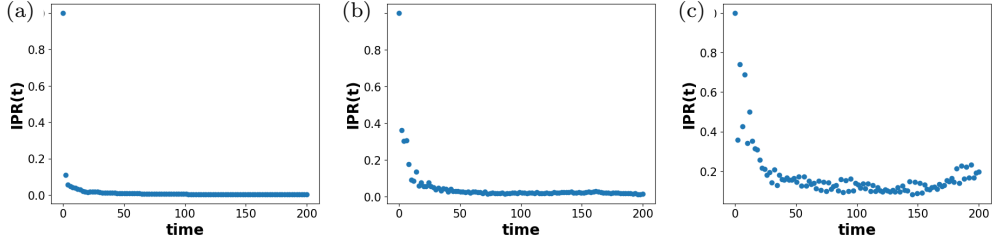

FIG. 13: (a), (b), (c) are the plots of IPR as a function of time for $\lambda = 0.5$, 2, 4 respectively for system size L = 1002 and $\nu = 0.908$

t can be expressed as follows[45]:

$$\sigma^2(t) = \sum_n (n - m)^2 |\psi_n(t)|^2. \qquad (7)$$

The dependence of MSD on time shows power law behavior [45], so $\sigma^2(t)$ goes as t^μ. Depending upon the different μ values, the dynamics of the wave packet can be characterized as follows: If the value is $\mu = 1$, then the region will be called ordinary diffusion; if the value is, $1 < \mu < 2$ then the phase can be called super diffusion, and if the value is, $\mu = 2$ then the region can be called ballistic [46, 47]. On the other hand, if $\mu = 0$, then the wave function can be called to be localized, whereas, $0 < \mu < 1$ represents subdiffusive motion [48–50].

In both the ν values, we have calculated mean-square displacement at those points by taking the 1002 system size at different modulation strengths $\lambda = 0.5$, 2, and 4 points, respectively, in Fig. 10 and 11. In our calculation, we have considered that at time $t = 0$; the electron starts at the 501th (middle) site. By calculating MSD, we can measure the deviation of the electron from its initial position at any later time. For modulation strength $\lambda = 0.5$, all states are extended in nature; in that region, we got the MSD to vary as $\sigma^2 \propto t^{2.02}$ (Fig. 10) for $\nu = 0.908$, in the same λ value the picture is same for $\nu = 1$. This represents that the motion of the electron's ground state wave function is ballistic at $\lambda = 0.5$ for both $\nu = 0.908$ and $\nu = 1$. For $\lambda = 2$, and $\nu = 0.908$ the MSD varies as follows: $\sigma^2 \propto t^{1.55}$ representing that the electronic

motion behaves super diffusively. For large distortion strength $\lambda = 4$, the MSD at limit $\nu = 0.908$ varies as t^1, which means the motion is still in the ordinary diffusion region. So here we can see for $\nu = 0.908$ point, even if the distortion modulation is high enough, the system is not completely localized (t^0). However, for $\nu = 1$ at $\lambda = 2$, the MSD varies as $t^{1.1}$, which is superdiffusive or near to ordinary diffusivity, a clear indication of criticality. As the distortion strength is increased a little beyond $\lambda = 2$, all the states are getting localized (Fig. 6e, 6f); as a result, the MSD is becoming time-independent, and the fluctuation is also very high. The transition of MSD time exponent with distortion strength (λ) at points $\nu = 0.908$ and $\nu = 1$ is shown in Fig. 15. For the robustness of the three different phases in both $\nu = 0.908$ and $\nu = 1$, the behavior of MSD at a very large time has been studied in Fig. 12. We can see $\nu = 0.908$ for all the values of λ; the electronic wave function does not show localization (t^0). But for $\nu = 1$ at $\lambda = 4$, a complete localization is observed.

B. Time dependent IPR

In this section, we will talk about the time dependence of the IPR on the system's evolution over time. The time-dependent IPR can be defined as follows:
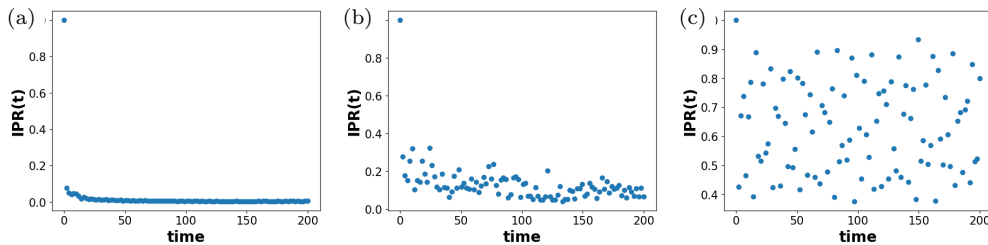
$$IPR(t) = \sum_n |\psi_n(t)|^4 \qquad (8)$$

FIG. 14: (a), (b), and (c) are the plots of IPR as a function of time for λ =0.5, 2, 4 respectively, for system size 1002 and $\nu = 1$
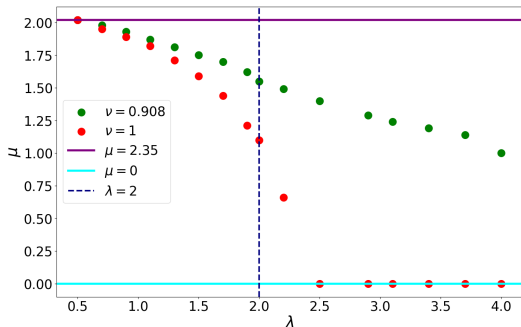

FIG. 15: μ vs. λ

where n represents the atomic site index. At time t=0, if the particle is at m^{th} site, then at time t=0 we will have $|\psi_m(t=0)|^4 = 1$ and $|\psi_{n \neq m}(t=0)|^4 = 0$. That is, $IPR(t=0)$ is always unity irrespective of whether the state is delocalized, localized, or mixed. The wave packet will be displaced from its initial position with a non-zero probability $|\psi_n(t)|^2$ on each site if the state starts delocalizing. As a result, the amplitude $|\psi_n(t)|^2$ decreases with time on each site. Over time, the sum of the $|\psi_n(t)|^4$ over atomic sites will tend to be zero. The wave packet is limited to the area close to the initial position during the localization. The probability $|\psi_n(t)|^2$ is large around the localization sites and zero on other sites. For this kind of wave function distribution on the sites, the IPR(t) never equals zero at even a large time. We have shown the time variation of IPR(t) for different distortion modulation strengths in Fig. 13 for $\nu = 0.908$ with system size L = 1002. In Fig. 13, we can see that at $\lambda = 0.5$ for a long time, it immediately goes to zero as time starts (just after t = 0). IPR for the critical point ($\lambda = 2$) at $\nu = 0.908$ goes to zero after a finite time (later time than at $\lambda = 0.5$). For $\lambda = 4$, it does not reach zero completely, and after some time, it shows little increase, representing that there is no complete localization (or presence of mixed states). As a result, the IPR will oscillate between small finite values even after a long time. But on the other hand, the IPR has been studied for $\lambda = 0.5, 2,$ 4 respectively (Fig. 14) at the limit $\nu = 1$, we can see the IPR goes to zero immediately after switching on time for $\lambda = 0.5$; however, for $\lambda = 2$ (at the critical point), IPR

oscillates in a short time region and eventually goes to zero with little fluctuation. Finally, at $\lambda = 4$, the IPR is always very high (close to 1) at a later time than $t = 0$, representing complete localization. We have also studied how the IPR varies with time for a critical value of distortion strength (λ) Fig. 16 with different system sizes. For smaller system sizes, L = 602, the IPR(t) oscillates and takes finite values as time progresses, representing the emergence of small localization of the wave packet. For L = 802 and L = 1002, the IPR(t) reaches zero without oscillation at long times, representing the presence of pure delocalized states.

C.   Return probability (RP)

Considering the wave packet to be at position m at time $t = 0$, the probability of finding the particle at its initial position can be expressed as:

$$P_m(t) = |\psi_m(t)|^2.$$

This is called the return probability (RP). If after a long time t, the RP remains non-zero at its initial site, then it represents the wave packet is localized at its initial site. On the other hand, if the wave packet spreads away from its initial position, then the RP vanishes with time. In our calculation, we have considered that the wave packet is exactly at 501th position at time $t = 0$. In Fig. 17 we have demonstrated the RP at different distortion strength $\lambda = 0.5$, 2 and 4 respectively for $\nu = 0.908$ point for system size L = 1002. We can see that at $\lambda = 0.5$, the wave packet will spread completely over the atomic sites. As a result, the return probability will go to zero for a long time [51]. Almost the same kind of property can be seen for $\lambda = 2$, but at the intermediate time, it shows a nonzero spike representing the emergence of localization of the wave packet at that particular distortion strength (criticality). After that, for $\lambda = 4$, we see the probability of finding the wave packet at 501th site oscillates with time, but it never goes to zero. The wave packet is not fully localized but can spread to nearby sites. On the other hand, for $\nu = 1$ (Fig. 18) at $\lambda = 0.5$, RP goes to zero immediately after switching the time on. At the critical point $\lambda = 2$, RP decreases from the value unity
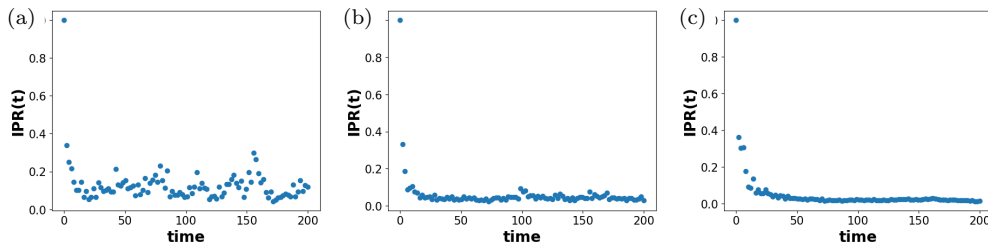
FIG. 16: (a), (b), and (c) are the plots of IPR as a function of time for critical value $\lambda = 2$ for system size L = 602, 802, and 1002, respectively, in limit $\nu = 0.908$
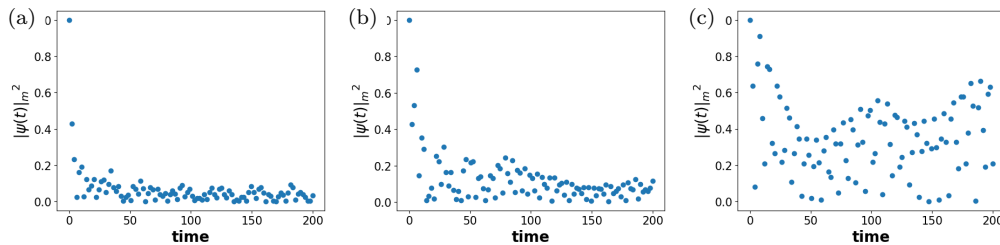

FIG. 17: (a), (b), and (c) are the plots of return probability as a function of time for $\lambda = 0.5$, 2, and 4, respectively, for system size = 1002 and $\nu = 0.908$

but remains almost constant over time. At large distortion strength $\lambda = 4$, RP always remains close to unity, describing strong localization.

D. Shannon / Information entropy (IE) Entropy

In this section, we will discuss delocalization and localization in light of information entropy or Shannon entropy. Shannon entropy can be expressed as follows:

$$S(t) = -\sum_n P_n log(P_n). \qquad (9)$$

In the above equation P_n suggests the probability of finding the particle at n^{th} site at time t. Thus P_n can be expressed as $P_n = |\psi_n(t)|^2$ so that $0 \leq P_n \leq 1$ and $\sum_n P_n = 1$. In Fig. 19, we have studied the information entropy as a function of time for different system sizes at the critical value of distortion strength $\lambda = 2$ and at $\nu = 0.908$. The first thing to notice here is that the information entropy is a monotonic function of time at a very early time region. After that, the entropy saturates because of the finiteness of the system size. The initial monotonic increase is because of the delocalization of the wave packet. Here, as the system size increases, the saturation time increases as the wave packet needs more time to completely spread on the Hilbert space, and the value of entropy at which it saturates also increases. For the $L = 602$ size of the system, we can see some oscillation in the entropy graph representing the effect of localization at a smaller system size. However, as the system size increases for $L = 802$ and $L = 1002$, the os-

cillation (fluctuations) of the entropy decreases. In Fig. 20, we have studied information entropy of system size $L = 1002$ at different distortion strengths $\lambda = 0.5$, 2, and 4 for $\nu = 0.908$ limit. We can see that for $\lambda = 0.5$, the system has IE monotonically increasing with time and then having saturation. When we increase the λ value to 2, the wave packet retains its initial monotonic increase region with saturation later with little fluctuation. In the case of $\lambda = 4$, IE still retains the monotonic increase in a comparatively small time limit, but the fluctuation is larger than the case in $\lambda = 4$, representing the presence of mixed states. As we know, for the region of localization, the states will be localized to a small region of the atomic sites, and the wave packet will only spread among that small region. As a result, although we will see a small increase in IE at a small time range, it will reach saturation faster with a lower entropy value. At the end, we also have studied IE at $\nu = 1$ (Fig. 21) at different λ limits. IE at $\lambda = 0.5$ goes to saturation after an initial monotonic growth with time. At the critical point $\lambda = 2$, IE has a very small time-dependent part, and the fluctuation has also increased. At $\lambda = 4$, IE goes as t^0 with time with larger fluctuation representing strong localization. For a better understanding of the entropy in the system, we also plotted the IE within the long time limits for both the values of ν. In Fig. 22, we can see the entropy of the wave packet saturates after an initial increase with time. For $\nu = 0.908$ and 1, the entropy saturates with the same entropy value at $\lambda = 0.5$. However, when the lambda is increased to $\lambda = 2$, the fluctuation is larger for $\nu = 1$ compared to that of the $\nu = 0.908$. For $\lambda = 4$, no time dependence of entropy can be seen for $\nu = 1$, and the fluctuation is very high, and the entropy
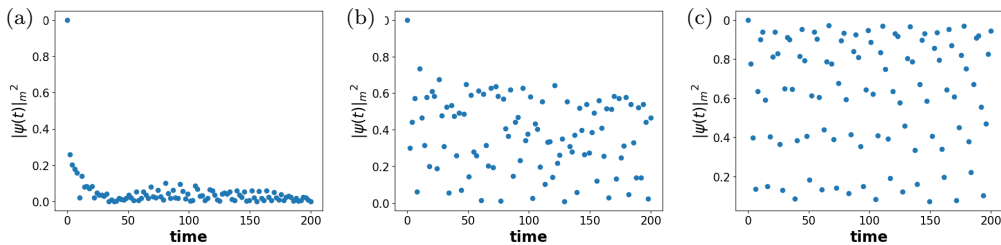
FIG. 18: (a), (b), and (c) are the plots of return probability as a function of time for $\lambda = 0.5$, 2, and 4, respectively, for system size = 1002 and $\nu = 1$

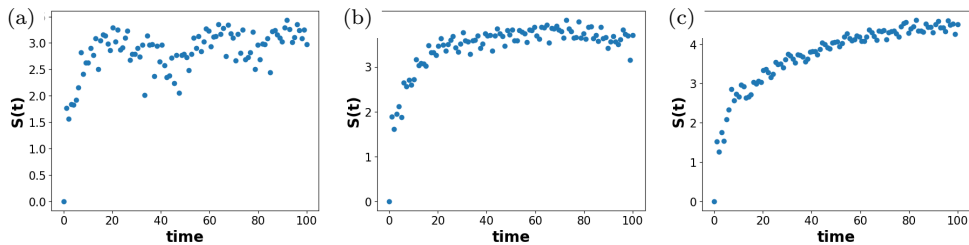FIG. 19: ((a), (b), and (c) are the plots of Shannon Entropy as a function of time for critical value $\lambda = 2$ for system size L = 602, 802, and 1002, respectively for $\nu = 0.908$

is very low as the wave packet will remain localized at its initial position at all instants. But in $\nu = 0.908$, even at $\lambda = 4$, there is a time dependence in entropy with comparatively less fluctuation. And entropy saturates with a larger value, compared to the case of $\nu = 1$.

V. CONCLUSION

We have done an extensive study on the eigenstate, multi- fractality, and quantum dynamics of a wave packet inside a ladder quantum network with a constant horizontal hopping parameter and a slowly varying generalized AAH kind of aperiodic vertical hopping with a general exponent term at its three different values: ν =0.6, 0.908, and 1. Our analysis shows the metal-insulator transition depending on the strength of the AAH modulation, which is applied as the vertical hopping. We have demonstrated the phase diagram of the ladder network in ν-λ parameter space. Our main finding in this paper is that we have seen that the intermediate value of $\nu = 0.908$, a perfect metal-to-insulator phase transition, is not possible. Due to the presence of SPME, the energy region near the center remains delocalized even at higher distortion strength. Apart from these, it also shows a multifractal character near their transition point (critical region) for both $\nu = 0.908$ and $\nu = 1$. We also have studied the quantum dynamics of the wave packet for this particular network at $\nu = 0.908$ different modulation strengths of λ =0.5, 2, and 4, which show different characters than the regular ladder network (with $\nu = 1$ limit). The long-time behavior of mean square displacement signifies that it is obvious that the wave packet motion at $\nu = 0.908$

is not entering into localization even at strong distortion strength ($\lambda = 4$). The results we got for return probability and the corresponding time-dependent inverse participation ratio are in good agreement with the results of the MSD calculation. As discussed in detail, $\lambda = 0.908$, the network exhibits a ballistic and, after that, ordinary diffusive (or very close to it) character under even high modulation strength applied as the vertical hopping. As the near central energy region at $\nu = 0.908$, this network shows an extended nature even at strong modulation strength, the wave packet contains localized and delocalized parts. As a result, the time evolution of the delocalized part of the wave packet spreads out, but the localized part of the wave packet still remains at the site of release (at $t = 0$). The behavior of the delocalized part of the wave packet can be mainly observed through the long-time behavior of the MSD. The initial site's amplitude never affects the MSD calculation. In general, if a system shows ballistic motion, the return probability is always zero as the wave packet moves throughout the system, and the corresponding inverse participation ratio also immediately goes to zero as time switches on. But in the limit $\nu = 0.908$ case, the localized part of the wave packet still remains in the initial location after a long time; as a result, the system has a finite return probability when the system enters its mixed region (both delocalized and localized states), and the corresponding IPR never decays exactly to zero(even increases at a later time). We can, therefore, conclude that the quantum dynamics of mixed states have a unique character; the localized portion of the wave packet controls the information entropy, return probability, and time-dependent inverse participation ratio, while the delocalized portion
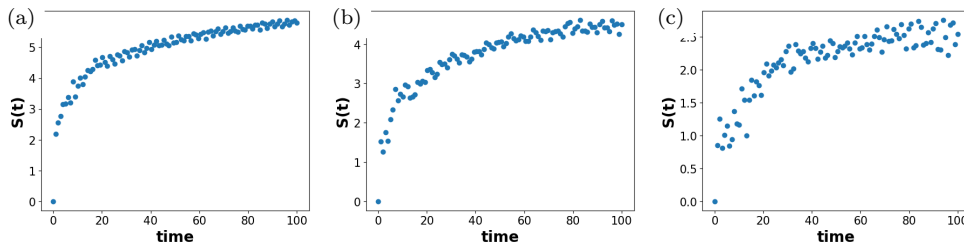
FIG. 20: (a), (b), and (c) are the plots of Shannon entropy as a function of time for $\lambda = 0.5$, 2, and 4, respectively, for system size L = 1002 for $\nu = 0.908$
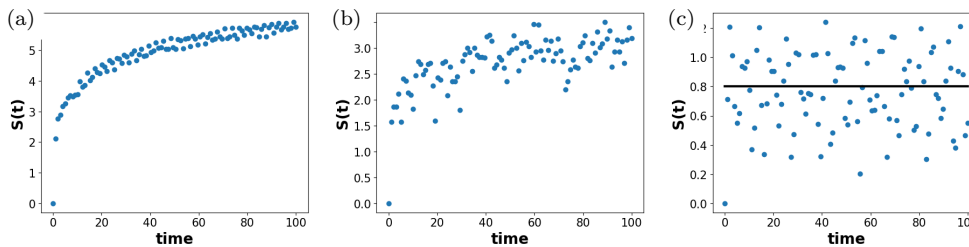

FIG. 21: (a), (b), and (c) are the plots of Shannon entropy as a function of time for $\lambda = 0.5$, 2, and 4, respectively, for system size L = 1002 for $\nu = 1$.

of the wave packet controls the MSD.

VI.   APPENDIX

In Fig. 4 (IPR vs. ν), we can see two major dips in the plot. We have thoroughly investigated the $\nu = 0.908$ (first dip), and the point $\nu = 0.97$ (second dip) has a comparatively larger number of delocalized states even in the higher disorder strength (λ). The IPR results are shown in Fig. 23. In the case of $\nu = 0.97$, the behavior of the wave packet is more or less the same. The MSD, in this case, will increase with a larger exponent in the higher distortion strengths (Fig. 24).

[1] S. Aubry and G. André, Analyticity breaking and anderson localization in incommensurate lattices, Proceedings, VIII International Colloquium on Group-Theoretical Methods in Physics **3** (1980).

[2] Z. M. Stadnik, *Physical Properties of Quasicrystals* (Springer Berlin, Heidelberg, 1998).

[3] J. B. Sokoloff, Band structure and localization in incommensurate lattice potentials, Phys. Rev. B **23**, 6422 (1981).

[4] S. Das Sarma, S. He, and X. C. Xie, Mobility edge in a model one-dimensional potential, Phys. Rev. Lett. **61**, 2144 (1988).

[5] J. Biddle and S. Das Sarma, Predicted mobility edges in one-dimensional incommensurate optical lattices: An exactly solvable model of anderson localization, Phys. Rev. Lett. **104**, 070601 (2010).

[6] Y. E. Kraus, Y. Lahini, Z. Ringel, M. Verbin, and O. Zilberberg, Topological states and adiabatic pumping in quasicrystals, Phys. Rev. Lett. **109**, 106402 (2012).

[7] X. Cai and Y.-C. Yu, Exact mobility edges in quasiperiodic systems without self-duality, Journal of Physics: Condensed Matter **35**, 035602 (2022).

[8] C. Aulbach, A. Wobst, G.-L. Ingold, P. Hänggi, and I. Varga, Phase-space visualization of a metal–insulator transition, New Journal of Physics **6**, 70 (2004).

[9] T. Liu and X. Xia, Real-complex transition driven by quasiperiodicity: A class of non-$\mathcal{PT}$ symmetric models, Phys. Rev. B **105**, 054201 (2022).

[10] T. Liu and S. Cheng, Mobility edges generated by the non-hermitian flatband lattice, Chinese Physics B **32**, 027102 (2023).

[11] S. Longhi, Phase transitions in non-hermitian superlattices, Phys. Rev. B **107**, 134203 (2023).

[12] M. Johansson and R. Riklund, Self-dual model for one-dimensional incommensurate crystals including next-nearest-neighbor hopping, and its relation to the hofstadter model, Phys. Rev. B **43**, 13468 (1991).
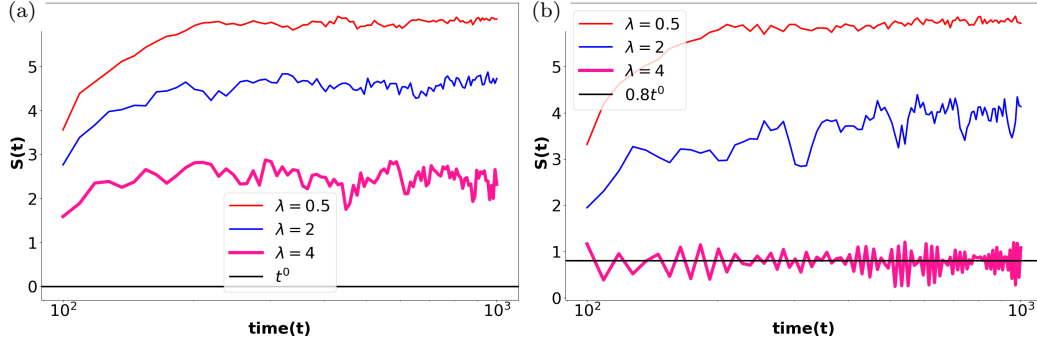
FIG. 22: (a), (b) are the plots of Shannon entropy as a function of (long) time for $\nu = 0.908$, $\nu = 1$ respectively
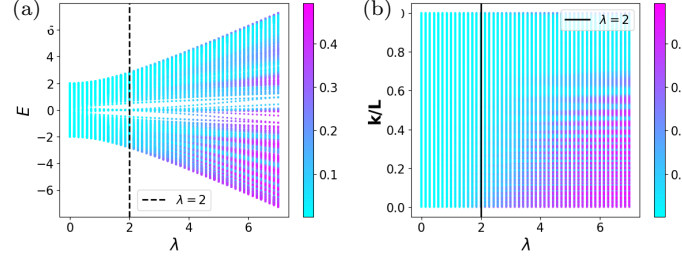

FIG. 23: IPR density a function of (a) energy and distortion strength (λ) (b) normalized index and distortion strength (λ)
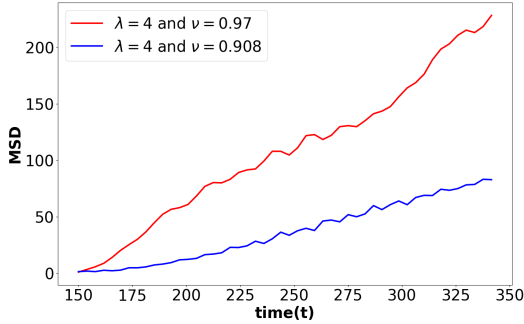

FIG. 24: Long time behavior of MSD for $\nu = 0.908$ and $\nu = 0.97$ at $\lambda = 4$

[13] M. Yahyavi, B. Hetényi, and B. Tanatar, Generalized aubry-andré-harper model with modulated hopping and p-wave pairing, Phys. Rev. B **100**, 064202 (2019).

[14] F. A. An, K. Padavić, E. J. Meier, S. Hegde, S. Ganeshan, J. H. Pixley, S. Vishveshwara, and B. Gadway, Interactions and mobility edges: Observing the generalized aubry-andré model, Phys. Rev. Lett. **126**, 040603 (2021).

[15] F. A. An, E. J. Meier, and B. Gadway, Engineering a flux-dependent mobility edge in disordered zigzag chains, Phys. Rev. X **8**, 031045 (2018).

[16] H. P. Lüschen, S. Scherg, T. Kohlert, M. Schreiber, P. Bordia, X. Li, S. Das Sarma, and I. Bloch, Single-particle mobility edge in a one-dimensional quasiperiodic optical lattice, Phys. Rev. Lett. **120**, 160404 (2018).

[17] Y. Lahini, R. Pugatch, F. Pozzi, M. Sorel, R. Morandotti, N. Davidson, and Y. Silberberg, Observation of a localization transition in quasiperiodic photonic lattices, Phys. Rev. Lett. **103**, 013901 (2009).

[18] V. Goblot, A. Strklj, N. Pernet, J. Lado, C. Dorow, A. Lematite, L. Le Gratiet, A. Harouri, I. Sagnes, and S. Raverts et al, Emergence of criticality through a cascade of delocalization transitions in quasiperiodic chains, Nat. Phys. **16**, 832 (2020).

[19] Y. Li, H.and Wang and Y. e. a. Shi, Observation of critical phase transition in a generalized aubry-andré-harper model with superconducting circuits, npj Quantum Inf **9**, 40 (2023).

[20] N. Mott, The mobility edge since 1967, Journal of Physics C: Solid State Physics **20**, 3075 (1987).

[21] S. Ganeshan, J. H. Pixley, and S. Das Sarma, Nearest neighbor tight binding models with an exact mobility edge in one dimension, Phys. Rev. Lett. **114**, 146601 (2015).

[22] Y. Wang, J.-H. Zhang, Y. Li, J. Wu, W. Liu, F. Mei, Y. Hu, L. Xiao, J. Ma, C. Chin, and S. Jia, Observation of interaction-induced mobility edge in an atomic aubry-andré wire, Phys. Rev. Lett. **129**, 103401 (2022).

[23] T. Liu, H. Guo, Y. Pu, and S. Longhi, Generalized aubry-andré self-duality and mobility edges in non-hermitian quasiperiodic lattices, Phys. Rev. B **102**, 024205 (2020).

[24] T. Liu, S. Cheng, H. Guo, and G. Xianlong, Fate of majorana zero modes, exact location of critical states, and unconventional real-complex transition in non-hermitian quasiperiodic lattices, Phys. Rev. B **103**, 104203 (2021).

[25] S. Biswas, Two-strand ladder network variants: Localization, multifractality, and quantum dynamics under an aubry-andré-harper kind of quasiperiodicity, Physica B: Condensed Matter , 416705 (2024).

[26] I. V. Gornyi, A. D. Mirlin, and D. G. Polyakov, Interacting electrons in disordered wires: Anderson localization and low-t transport, Phys. Rev. Lett. **95**, 206603 (2005).

[27] D. Basko, I. Aleiner, and B. Altshuler, Metal–insulator transition in a weakly interacting many-electron system with localized single-particle states, Annals of Physics **321**, 1126 (2006).

[28] V. Oganesyan and D. A. Huse, Localization of interacting fermions at high temperature, Phys. Rev. B **75**, 155111 (2007).

[29] M. Žnidarič, T. c. v. Prosen, and P. Prelovšek, Many-body localization in the heisenberg xxz magnet in a random field, Phys. Rev. B **77**, 064426 (2008).

[30] A. Pal and D. A. Huse, Many-body localization phase transition, Phys. Rev. B **82**, 174411 (2010).

[31] J. H. Bardarson, F. Pollmann, and J. E. Moore, Unbounded growth of entanglement in models of many-body localization, Phys. Rev. Lett. **109**, 017202 (2012).

[32] J. M. Deutsch, Quantum statistical mechanics in a closed system, Phys. Rev. A **43**, 2046 (1991).

[33] M. Srednicki, Chaos and quantum thermalization, Phys. Rev. E **50**, 888 (1994).

[34] P. Bordia, H. P. Lüschen, S. S. Hodgman, M. Schreiber, I. Bloch, and U. Schneider, Coupling identical one-dimensional many-body localized systems, Phys. Rev. Lett. **116**, 140401 (2016).

[35] Y.-L. Wu and S. Das Sarma, Understanding analog quantum simulation dynamics in coupled ion-trap qubits, Phys. Rev. A **93**, 022332 (2016).

[36] R. Modak and S. Mukerjee, Many-body localization in the presence of a single-particle mobility edge, Phys. Rev. Lett. **115**, 230401 (2015).

[37] H. P. Lüschen, P. Bordia, S. Scherg, F. Alet, E. Altman, U. Schneider, and I. Bloch, Observation of slow dynamics near the many-body localization transition in one-dimensional quasiperiodic systems, Phys. Rev. Lett. **119**, 260401 (2017).

[38] P. Bordia, H. Lüschen, S. Scherg, S. Gopalakrishnan, M. Knap, U. Schneider, and I. Bloch, Probing slow relaxation and many-body localization in two-dimensional quasiperiodic systems, Phys. Rev. X **7**, 041047 (2017).

[39] A. Rubio-Abadal, J.-y. Choi, J. Zeiher, S. Hollerith, J. Rui, I. Bloch, and C. Gross, Many-body delocalization in the presence of a quantum bath, Phys. Rev. X **9**, 041014 (2019).

[40] X. Li, S. Ganeshan, J. H. Pixley, and S. Das Sarma, Many-body localization and quantum nonergodicity in a model with a single-particle mobility edge, Phys. Rev. Lett. **115**, 186601 (2015).

[41] X. Li, J. H. Pixley, D.-L. Deng, S. Ganeshan, and S. Das Sarma, Quantum nonergodicity and fermion localization in a system with a single-particle mobility edge, Phys. Rev. B **93**, 184204 (2016).

[42] W. De Roeck, F. Huveneers, M. Müller, and M. Schiulaz, Absence of many-body mobility edges, Phys. Rev. B **93**, 014203 (2016).

[43] S. Nag and A. Garg, Many-body mobility edges in a one-dimensional system of interacting fermions, Phys. Rev. B **96**, 060203 (2017).

[44] D. R. Grempel, S. Fishman, and R. E. Prange, Localization in an incommensurate potential: An exactly solvable model, Phys. Rev. Lett. **49**, 833 (1982).

[45] D. Katsanos, S. Evangelou, and S. Xiong, Quantum electron dynamics in periodic and aperiodic sequences, Physical Review B **51**, 895 – 904 (1995), cited by: 32.

[46] S. Biswas and A. Chakrabarti, Engineering complete delocalization of single particle states in a class of one dimensional aperiodic lattices: A quantum dynamical study, Physica E: Low-dimensional Systems and Nanostructures **162**, 116010 (2024).

[47] A. Maity and A. Chakrabarti, Engineering insulator-metal transition in a class of decorated aperiodic lattices: A quantum dynamical study, Physics Letters A **406**, 127452 (2021).

[48] P. Siegle, I. Goychuk, and P. Hänggi, Origin of hyperdiffusion in generalized brownian motion, Phys. Rev. Lett. **105**, 100602 (2010).

[49] J. Vollmer, L. Rondoni, M. Tayyab, C. Giberti, and C. Mejía-Monasterio, Displacement autocorrelation functions for strong anomalous diffusion: A scaling form, universal behavior, and corrections to scaling, Physical Review Research **3**, 10.1103/PhysRevResearch.3.013067 (2021).

[50] A. Bodrova, A. K. Dubey, S. Puri, and N. Brilliantov, Intermediate regimes in granular brownian motion: Superdiffusion and subdiffusion, Phys. Rev. Lett. **109**, 178001 (2012).

[51] C. Guan and X. Guan, A brief introduction to anderson localization (2019).

[52] X. Li and S. Das Sarma, Mobility edge and intermediate phase in one-dimensional incommensurate lattice potentials, Phys. Rev. B **101**, 064203 (2020).